PAPER • OPEN ACCESS

Phase decomposition and nano structure evolution of metastable nanocrystalline Cu-Co solid solutions during thermal treatment

To cite this article: A Bachmaier *et al* 2015 *IOP Conf. Ser.: Mater. Sci. Eng.* **89** 012017

View the article online for updates and enhancements.

Related content

- Formation of -Phase in $Fe_{66}Nb_{10}B_{30}$ Amorphous Alloy with a Large Supercooled Liquid Region

- Cu-Co-Ni alloys: an efficient and durable electrocatalyst in acidic media

- Nano structure evolution in $P3HT:PC_{61}BM$ blend films due to the effects of thermal annealing or by adding solvent

Recent citations

- Microstructure Evolution and Mechanical Stability of Supersaturated Solid Solution Co-Rich Nanocrystalline Co-Cu Produced by Pulsed Electrodeposition
Killang Pratama *et al*

- Thermal stability, phase decomposition, and micro-fatigue properties of pulsed electrodeposited nanocrystalline Co-Cu
K. Pratama *et al*

Phase decomposition and nano structure evolution of metastable nanocrystalline Cu-Co solid solutions during thermal treatment

A Bachmaier[1], M Stolpe[2], T Müller[1,3] and C Motz[1]

[1] Chair of Materials Science and Methods, Campus D2.2, Saarland University, Saarbrücken, Germany
[2] Metallic Materials, Campus C6.3, Saarland University, Saarbrücken, Germany
[3] Erich Schmid Institute of Materials Science, Austrian Academy of Science, Jahnstraße 12, Leoben, Austria

E-mail: a.bachmaier@matsci.uni-sb.de

Abstract. Nanocrystalline and ultrafine-grained $Cu_{100-x}Co_x$ (x =26 and 76) solid solutions have been prepared by severe plastic deformation (SPD) of elemental powder mixtures. For both concentrations a supersaturated solid solution fcc phase was identified after the deformation process with grain sizes of less than 50 nm for Co rich solutions and around 100 nm for Cu rich solutions. Additionally, synthesis of nanocrystalline materials in the Cu-Co alloy system by electrodeposition has been conducted. Microstructural characterization by scanning and transmission electron microscopy, differential scanning calorimetry, and microhardness measurements are used to investigate the structural evolution, the thermal stability and mechanical properties of the different nanocrystalline Cu-Co alloy materials during isothermal and non-isothermal annealing. In this study it is shown that the phase decomposition of the metastable Cu-Co solid solutions has a significant influence on their thermal stability, which can be linked to the underlying microstructure that forms during annealing.

1. Introduction

Nanocrystalline (nc) and ultrafine-grained (ufg) materials have been a subject of extensive research over the past couple of decades due to their extraordinary mechanical and physical properties like high strength [1-3]. Nc and ufg materials are, however, thermally and mechanically unstable due to the large amount of enthalpy stored in their large grain boundary area, and structural coarsening affects material properties considerably even for annealing at low temperatures for short times [4]. Hence, the stability of nc and ufg materials is a fundamental issue, but strategies to enhance grain size stability are still under research.

In this study, synthesis of bulk nc and ufg materials is conducted by severe plastic deformation (SPD) and electrodeposition (ED) in the Cu-Co model system. The peritectic Co-Cu system has a positive heat of mixing extending over the whole composition range and no room temperature solubility at all [5]. Due to strain-induced mechanical mixing, nc alloys with solubilities far beyond equilibrium have been already obtained in different immiscible Cu-based alloy systems by SPD [6-9]. In [10] it is reported, that Cu-Co solid solutions can be synthesized by ED as well. The metastable Cu-Co solid solutions are not in an equilibrium state after processing. During subsequent annealing treatments, phase decomposition is expected. Tailoring material properties for potential technological

applications requires an understanding of the structural changes which occur during annealing and an evaluation of a possible impact of phase decomposition on thermal stability and mechanical-physical properties. In this study, microstructural evolution during annealing and the thermal stability of electrodeposited and severe plastically deformed nc and ufg Cu-Co solid solutions are investigated. It is shown that the phase decomposition process has a major impact on the thermal stability with a direct relation of structure to stability.

2. Experimental

The initial two-phase $Cu_{100-x}Co_x$ materials (x=26 and 76 at. %) were hot-isostatically pressed at 900°C under vacuum by RHP-Technology (Seibersdorf, Austria) from Co powders (purity 99.9%) and Cu powders (purity 99.99%) into samples with a cylindrical shape and subsequently processed by SPD (high-pressure torsion (HPT) deformation at room temperature with a pressure of 5 GPa and a rotation speed of 0.2 rpm). To study the influence of the impurity content, Co and Cu powders with a lower purity (99.8 and 99.9%) were additionally prepared in the same composition by applying the same HPT deformation parameters. The strain value applied (equivalent strain ≥ 210 for a distance ≥ 1.5 mm from the sample centre) is high enough to obtain the steady state region of the microstructural refinement (i.e. further HPT deformation does not induce further grain refinement) in the samples [11,12].

Synthesis of $Cu_{24}Co_{76}$ alloys was further conducted by ED in reducing simultaneously the Cu^{2+} and Co^{2+} ions onto a Cu substrate from an electrolyte solution containing 112 g/l $CoSO_4 \cdot 7 H_2O$, 6 g/l $CuSO_4$, 142 g/l Na_2SO_4, 59 g/l $C_6H_5Na_3O_7 \cdot 2 H_2O$, 19 g/l H_3BO_3, 2g/l $C_7H_5NO_3S$ and 0.1 g/l $C_{12}H_{25}NaO_4S$ at 40°C. The deposition parameters were adjusted to obtain a Co content similar to the HPT deformed materials resulting in a current density j= − 30 mA/cm² at a pH= 4.5.

All samples were further subjected to isothermal heat treatments at 300°C, 400°C, 600°C for 1 h in air. Selected HPT deformed samples are also annealed at the same temperatures for 7 h and 100 h to investigate the long term stability of the processed materials. Vickers microhardness was measured on all samples in as-deformed/deposited and annealed conditions. Microstructural characterization was carried out by scanning electron microscopy (SEM) using a Zeiss SIGMA™-VP field emission SEM device. Electron-back scatter diffraction (EBSD) is conducted using the EBSD system (Oxford Nordlys EBSD detector) attached to the SEM and Oxford HKL Channel 5 analysis software. Transmission electron microscopy (TEM) investigations of selected samples were performed on a JEOL JEM 2011 instrument at an acceleration voltage of 200 kV.

Differential scanning calorimetry (DSC) and differential thermal analysis (DTA) measurements on selected samples were performed using a Perkin Elmer DSC 8000 and a Netsch STA 446/C/6/MFG/G Jupiter device. Subsequent re-runs served as the reference measurement and baseline for the analysis for all measurements. For the determination of the activation energies with the method of Kissinger, different linear heating rates of 10, 20, 60 and 120 °C/min in a temperature range from 25°C to 720°C were applied.

3. Results and Discussion

3.1. As-deformed state

Both Cu-Co alloy materials are deformed until the steady state is reached. During the HPT process, the microstructure of the initial two-phase Cu-Co materials is strongly refined. The microstructures of the alloys in this steady state are displayed in Figure 1, which shows SEM images recorded with back scattered electrons. Both samples are homogeneously refined. From the SEM images, it is not possible to distinguish between the Cu and Co phases. With increasing Co content in the alloy, the grain size is reduced. Similar types of nanostructures are obtained for the samples from the low-purity Cu-Co materials. Vickers hardness measurements reveal for both compositions the typical high hardness of HPT deformed materials. The hardness in the as-deformed state is 314±11 HV and 444±12 HV for the $Cu_{74}Co_{26}$ and $Cu_{24}Co_{76}$ alloy obtained from the high-purity material, respectively. The hardness of the

samples made of the lower-purity material is 281±4 HV ($Cu_{74}Co_{26}$) and 437±4 HV ($Cu_{24}Co_{76}$). All alloys exhibit a higher hardness compared to pure HPT deformed Cu and Co [13,14], which is due to the smaller grain size in the alloys compared to pure HPT deformed materials.
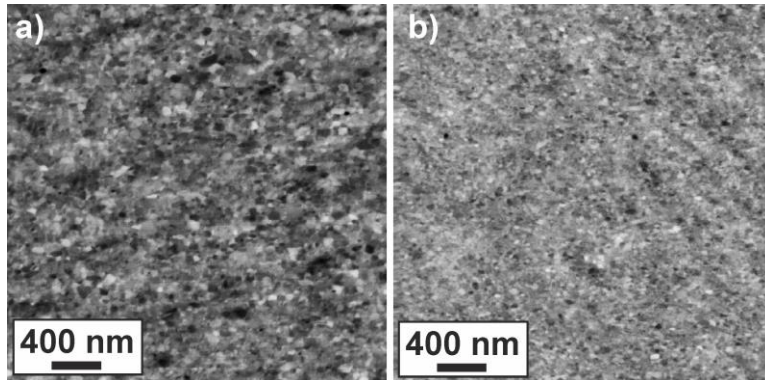

Figure 1: SEM images recorded with back-scattered electrons of the microstructure of the samples in the as-deformed condition: a) $Cu_{74}Co_{26}$ and b) $Cu_{24}Co_{76}$.

   Figure 2 shows bright-field TEM images of the as-deformed Co- and Cu-rich samples. From these images, a grain size less than 50 nm for Co rich alloy (Figure 2a) and around 100 nm for Cu rich alloy (Figure 2b) can be confirmed. In both selected area diffraction (SAD) patterns, a single set of diffraction rings is visible, which are either fcc Cu or fcc Co Debye-Scherrer rings of {111}, {200}, {220}, {311} and {222} planes. The fact that the fcc Cu and fcc Co Debye-Scherrer rings merge into each other might be explained by the formation of a supersaturated solid solution in the Cu-Co alloys. Due to the small difference in the lattice parameters of fcc Cu and fcc Co, a clear discrimination between the reflections from the SAD patterns is challenging. However, large supersaturations up to 26 at. % Co in fcc Cu have been recently confirmed by atom probe tomography (APT) in the $Cu_{74}Co_{26}$ alloy [15]. To prove the formation of supersaturated solid solutions in the alloys with a higher Co-content, APT investigations are currently conducted.
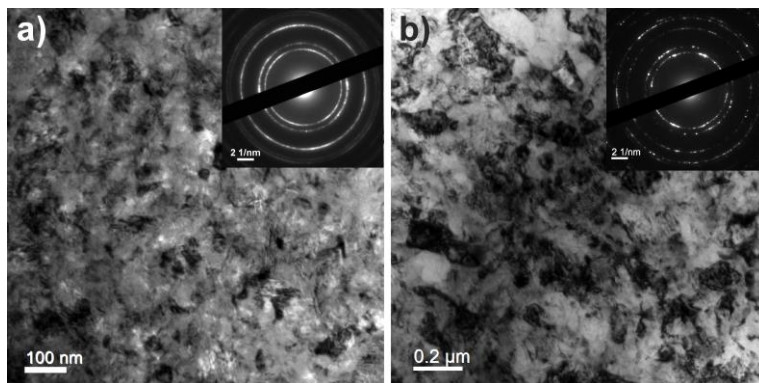

Figure 2: TEM bright field images with corresponding SAD patterns (insets) of the microstructure of the samples in the as-deformed condition: $Cu_{24}Co_{76}$ (a) and $Cu_{74}Co_{26}$ (b).

3.2. *As-deposited state*

Synthesis of bulk nc Cu-Co alloys is additionally conducted by ED. By adjusting the deposition parameters, a Cu-Co alloy with the same Co content as the HPT deformed Co-rich alloy ($Cu_{24}Co_{76}$) is obtained. Smaller Co contents similar to the composition of the HPT deformed Cu-rich alloy could not be achieved up to now. Figure 3a shows the microstructure of the as-deposited alloy recorded with back scattered electrons. Similar to the HPT deformed Co-rich alloys the grain size is nc and hardly resolvable by SEM. In Figure 3b, a bright-field TEM image with corresponding SAD pattern of the as-deposited Co-Cu alloy sample is shown. Only one set of fcc Debye-Scherrer rings (either fcc Cu or fcc Co) is observable in the SAD pattern, which also suggests a mixture of the two phases in the as-deposited condition. The ED Cu-Co alloy sample exhibits a quite high hardness in the as-deposited

state, which exceeds the hardness of the HPT deformed sample. The microhardness of the $Cu_{24}Co_{76}$ alloy is 471±9 HV.
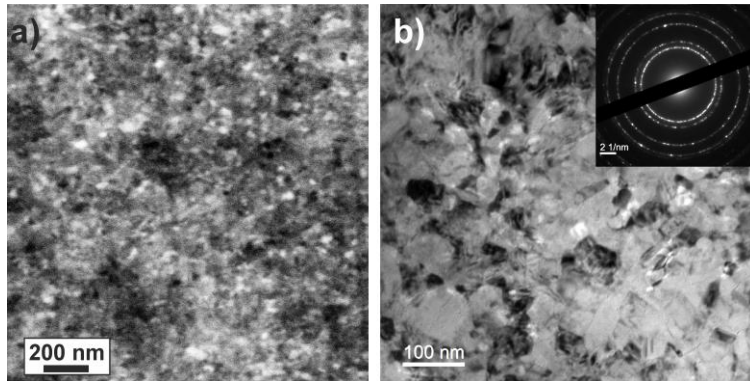

Figure 3: SEM image (a) recorded with back-scattered electrons and TEM bright field image (b) with corresponding SAD patterns (inset) of the microstructure of the $Cu_{24}Co_{76}$ alloy sample in the as-deposited condition.

3.3. Non-isothermal and isothermal annealing

To investigate the thermal stability of the Cu-Co alloys, the samples are initially annealed for 1h in air at three different temperatures (300°C, 400°C, 600°C), which corresponds to ~35, 40 and 52 % T_m with T_m being the melting temperature of the corresponding $Cu_{24}Co_{76}$ or $Cu_{74}Co_{26}$ alloys, respectively. The microhardness as a function of the annealing temperature after annealing for 1h in air is plotted in Figure 4. The microhardness of the HPT deformed $Cu_{24}Co_{76}$ alloy decreases only slightly for annealing temperatures up to 400°C. The hardness of the Cu rich alloy ($Cu_{74}Co_{26}$) even increases during annealing at the same temperatures. At the highest annealing temperature (600°C), a drop in hardness can be observed for both HPT deformed samples, which is less pronounced for the Co rich alloy. The microhardness of the ED $Cu_{24}Co_{76}$ alloy increases for the lowest annealing temperature (300°C) as well. However, at an annealing temperature of 400°C, a strong hardness decrease is observed (Δ HV = 133).
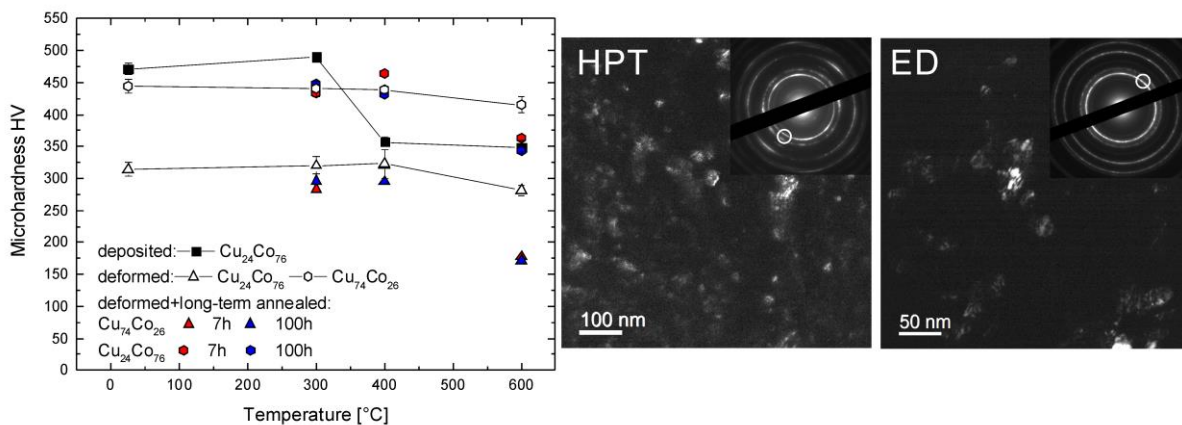

Figure 4: Microhardness of HPT deformed and ED Cu-Co alloy samples as a function of annealing temperature (300°C, 400°C, 600°C) after 1h annealing time. The microhardness of HPT deformed samples annealed at 300°C, 400°C and 600°C for 7 h and 100 h is also shown in the plot. Dark-field TEM images of the HPT deformed and ED $Cu_{24}Co_{76}$ alloy samples annealed for 1h at 300°C obtained by selecting the lattice reflections as indicated in the SAD patterns.

In Figure 4, dark-field TEM images of selected annealed microstructures (HPT deformed and ED $Cu_{24}Co_{76}$ alloy annealed for 1h at 300°C) are additionally shown. In both samples a nc structure is still visible. The corresponding SAD patterns (see insets) reflect the nc structure as well. Evaluation of the annealed microstructures by SEM after annealing at 400°C for 1h shows that the HPT deformed

Cu-Co alloys exhibit no distinct change compared to the microstructure in the as-deformed state. By contrast, massive grain growth occurs in the ED Cu$_{24}$Co$_{76}$ alloy (Figure 5a). Inside the micrometer-sized grains, a fine scaled substructure is visible (Figure 5b).

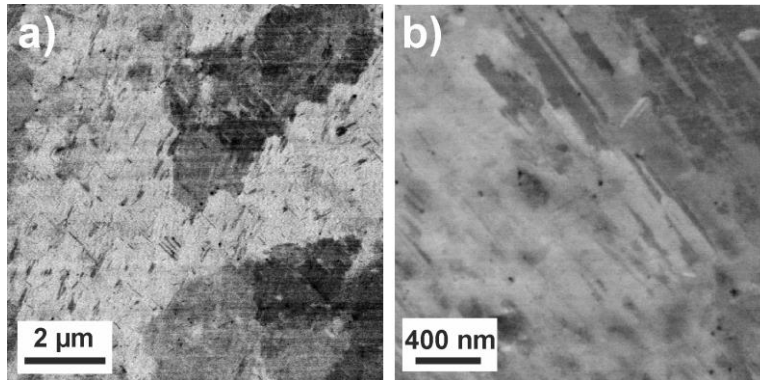**Figure 5:** SEM images recorded with back-scattered electrons of the microstructure of the ED Cu$_{24}$Co$_{76}$ alloy sample after annealing for 1h at 400°C: Overview (a) and detailed view with a high magnification (b).

Thermal analysis was further performed to determine the decomposition temperature and annealing kinetics of the HPT deformed Cu-Co alloy materials. The Cu$_{74}$Co$_{26}$ and Cu$_{24}$Co$_{76}$ alloy samples show broad and overlapping exothermic peaks in the DSC scans (Figure 6a and b). Overlapping peaks are reported to occur frequently during annealing of supersaturated solid solutions [16]. The thermal processes of the Cu-Co alloys are further not completed at the maximum temperature (720°C) which can be applied during the DSC measurements. Therefore, additional DTA measurements were carried out with a linear heating rate of 20 °C/minute in a temperature range from 25°C to 1000°C (Figure 6c). In these scans, additional broad exothermic peaks at higher temperatures are visible.
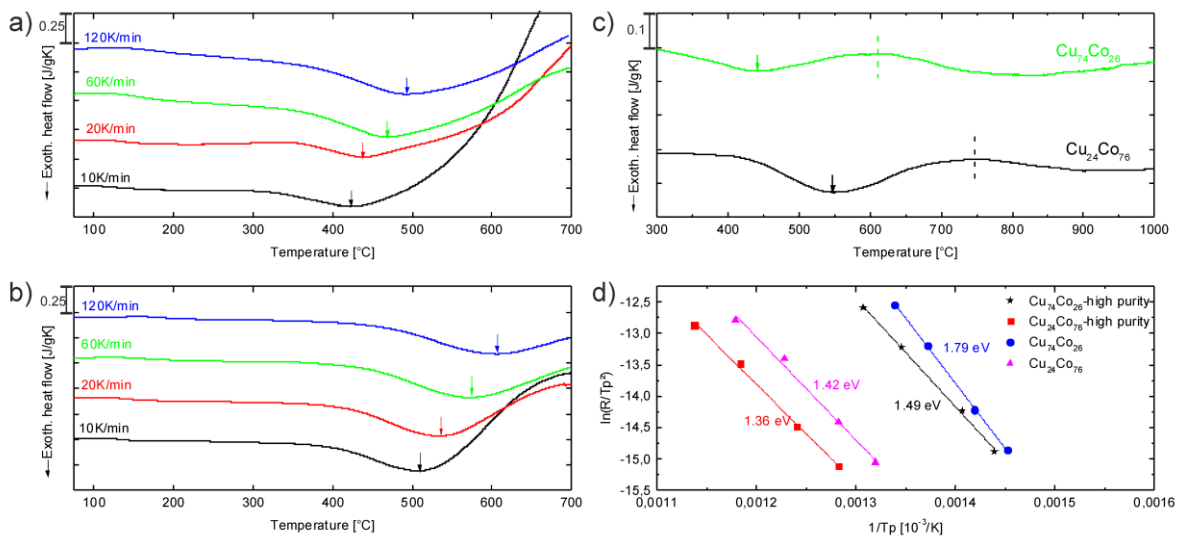

Figure 6: DSC scans with different heating rates for the Cu-Co alloys after HPT deformation: a) Cu$_{74}$Co$_{26}$ and b) Cu$_{24}$Co$_{76}$. DTA scans of both Cu-Co alloy samples with a heating rate of 20°C/minute (c). Kissinger plot for the Cu-Co alloy samples with different initial purities (d).

SEM microstructural characterization of the DSC samples heated up to 700°C shows no significant grain growth although distinct heat releases are clearly observable in the DSC scans (Figure 6a and b). On the contrary, SEM analysis shows that grain growth and phase decomposition take place in the Cu-Co alloy samples after the DTA scans (maximum temperature 1000°C). As an example, an EBSD phase map of the Cu$_{74}$Co$_{26}$ alloy sample after the DTA scan is displayed in Figure 7. Areas appearing red and blue in the map represent the fcc Cu phase and the hcp Co phase, respectively.
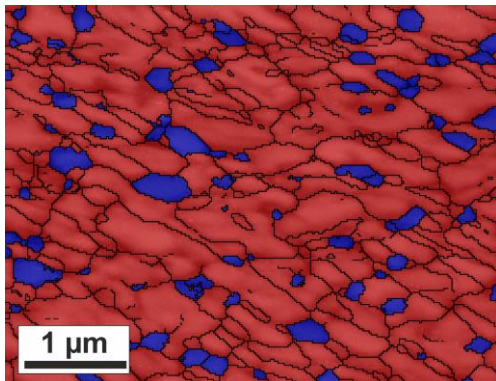
Figure 7: EBSD scan of the $Cu_{74}Co_{26}$ alloy sample after the DTA scan, with all grains belonging to the hcp Co and fcc Cu are marked as blue and red, respectively. The phase map is superimposed by an image quality map.

Hence, the exothermic peaks at intermediate temperatures (indicated by the arrows in the DSC and DTA scans) might be attributed to the decomposition process of the metastable Cu-Co solid solutions. With increasing Co content, the peak temperature of the decomposition process increases from ~440°C ($Cu_{74}Co_{26}$) to ~545°C ($Cu_{24}Co_{76}$). Additionally, the starting temperature of the second exothermic process (i.e. grain growth) is shifted to higher temperatures with increasing Co content (marked with dashed line in Figure 6c).

For the $Cu_{74}Co_{26}$ and $Cu_{24}Co_{76}$ alloy samples (low and high purity initial materials), the peak temperatures of the decomposition process at various heating rates are also evaluated by the method of Kissinger (Figure 6d). Due to the occurrence of broad and poorly separated peaks, the validity of the Kissinger analysis in terms of a single process is not strictly fulfilled and the obtained activation energies provide only a qualitative hint for the underlying processes occurring during phase decomposition. For the $Cu_{24}Co_{76}$ alloy samples, similar activation energies of 1.42±0.05eV (lower purity material) and 1.36±0.09eV (higher purity material) are determined. For the $Cu_{74}Co_{26}$ alloy samples, slightly different activation energies of 1.79±0.03eV (lower purity material) and 1.49±0.04eV (higher purity material) are observed. The value of activation energies for phase decomposition are considerably lower than values typical found for Co tracer diffusion in bulk Cu, 2.2 eV [17], Cu tracer diffusion in bulk Co, 2.85 eV, [18] and Co-Cu interdiffusion, 2.5 eV [19] and Cu and Co self-diffusion activation energies in the fcc lattice [20,21].

3.4. Long term stability
Selected samples are also annealed at 300°C, 400°C and 600°C for 7 h and 100 h to investigate the long term stability of the HPT processed materials. The measured microhardness after annealing is summarized in Table 1 and additionally plotted in Figure 4. At low annealing temperatures (300°C and 400°C), nearly no change in microhardness independent on annealing time is measured. In contrast, the microhardness decreases with increasing annealing time at the highest annealing temperature (600°C). After an annealing time of 7 h, a microhardness of 178±4 HV and 363±20 HV is measured for the $Cu_{74}Co_{26}$ and $Cu_{24}Co_{76}$ alloy, respectively. After 100h annealing time, the microhardness is further reduced to 171±3HV ($Cu_{74}Co_{26}$) and 343±13HV ($Cu_{24}Co_{76}$).

Long-term annealing at 400°C leads only to minor microstructural coarsening. Annealing at 600°C for different times results in notable coarsening instead. To give an example, TEM images of the $Cu_{74}Co_{26}$ alloy after annealing for 7h and 100h at 400°C and after annealing for 100h at 600°C are displayed in Figure 8. A grain size on the average around 100 nm is visible in the TEM bright field image of the microstructure annealed at 400°C for 7h (Figure 8a). Inside the grains, fine scaled contrast variations are additionally visible. Tilting the electron beam reveals that nearly all of the large grains show this kind of contrast modulations in the regions explored with TEM. In the SAD pattern, only fcc Debye-Scherrer rings of {111}, {200}, {220}, {311} and {222} planes are observed. Annealing for longer times at the same annealing temperature does not lead to further coarsening or to a significant change in the resulting microstructure (Figure 8b).

Table 1. Microhardness of annealed HPT processed samples.

microhardness	HPT $Cu_{74}Co_{26}$		HPT $Cu_{24}Co_{76}$	
annealed	7h	100h	7h	100h
300°C	283±10 HV	296±6 HV	433±7HV	448±8HV
400°C	320±12 HV	295±11 HV	464±13 HV	432±12 HV
600°C	178±4 HV	171±3HV	363±20 HV	343±13HV

On the contrary, the TEM bright field image of the $Cu_{74}Co_{26}$ alloy annealed for 100h at 600°C displays a microstructure in which significant grain growth occurred (Figure 8c). Similar modulated contrast variations as displayed in Figure 8a-b are visible in some of the grains. Some grains, however, fail to show any of these contrast variations. The SAD pattern shows two sets of spotty diffraction rings (fcc Cu and fcc Co) further confirming the observed microstructural coarsening.
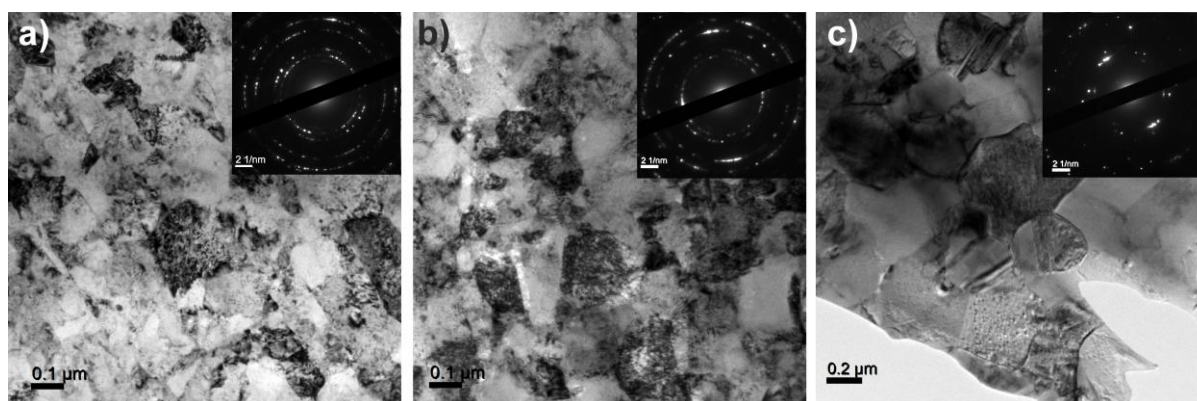

Figure 8: TEM bright field images with corresponding SAD patterns (insets) of the microstructure of the $Cu_{74}Co_{26}$ alloys after annealing for 7h (a) and 100 h (b) at 400°C and 100h at 600°C (c).

4. Summary
Nc and ufg bulk Cu-Co alloys have been prepared by HPT and ED with similar Co contents and their thermal stability during isothermal and non-isothermal annealing is investigated. The grain size and hardness in the as-deposited or as-deformed condition depends on the Co content. Samples with a higher Co content exhibit a higher hardness and smaller grain sizes. For both alloy compositions, the formation of fcc solid solutions is observed.

No significant grain growth is observed before completion of phase separation in the SPD-processed Cu-Co solid solutions. At intermediate annealing temperatures (≤400°C), the Cu-Co alloys are thermally stable even after annealing for several days. At the same time, a high hardness is maintained in the HPT deformed alloy materials. The onset temperature of phase separation is a function of the Co content and increases with increasing Co content. TEM investigations reveal that the vast majority of the grains at these temperature show modulated contrast variations which might indicate spinodal decomposition inside the grains.

For isothermal annealing at 600°C, phase separation and clearly visible microstructural coarsening is observed in the HPT deformed Cu-Co alloys. Although decomposition and microstructural coarsening cannot be hindered, an ufg structure is still maintained in the Cu-Co alloys even after annealing at 600°C (~50% Tm) for 100h. In principle, such phase decomposition mechanisms can be used to produce tailored nano structures to optimize e.g. thermal or mechanical properties.

Similarly, no significant change in the microstructure and microhardness is observed in the ED $Cu_{24}Co_{76}$ alloy sample annealed at 300°C. On the contrary, significant coarsening is observed in the ED alloy at an annealing temperature of 400°C. Inside the micrometer-sized grains, a fine-scaled substructure is observable, which might be responsible for the still quite high hardness of the ED Cu-Co alloy in the annealed state. The reasons for the differing behavior of electrodeposited and severe plastically deformed alloys is the scope of future work.

Acknowledgments

References
[1] Gleiter H 1989 *Prog. Mater. Sci.* **33** 223-315
[2] Gleiter H 2000 *Acta Mater.* **48** 1-29
[3] Meyers M A, Mishra A and Benson DJ 2006 *Prog. Mater. Sci.* **51(4)** 427-556
[4] Hibbard G, Aust KT, Palumbo G and Erb U 2001 *Scripta Mater.* **44** 513
[5] Nishizawa T and Ishida K 1984 *Bull. Alloy Phase Diagrams* **5** 161
[6] Sauvage X, Jessner P, Vurpillot F and Pippan R 2008 *Scripta Mater.* **58** 1125-28
[7] Bachmaier A, Rathmayr G B, Bartosik M, Apel D, Zhang Z and Pippan R 2014 *Acta Mater.* **69** 301-13
[8] Bachmaier A, Kerber M, Setman D and Pippan R 2012 *Acta Mater.* **60** 860
[9] Edwards D, Sabirov I, Sigle W and Pippan R 2012 *Phil. Mag.* **92** 4151–66
[10] Bran J, Jean M, Lardé R, Sauvage X, Le Breton JM, Morin-Grognet S and Pautrat A 2014 *J. Alloy Comp.* **596** 118-24
[11] Pippan R, Scheriau S, Taylor A, Hafok M, Hohenwarter A and Bachmaier A 2010 *Annu. Rev. Mater. Res.* **40** 319-43
[12] Hohenwarter A, Bachmaier A, Gludovatz B P, Scheriau S G and Pippan R 2009 *Int. J. Mater. Res.* **100** 1653-61
[13] Edalati K, Fujioka T and Horita Z 2008 *Mater. Sci. Eng. A* **497** 168–73
[14] Edalati K, Toh S, Arita M, Watanabe M and Horita Z 2013 *Appl. Phys. Letters* **102** 181902-1
[15] Bachmaier A, Aboulfadl H, Pfaff M, Mücklich F and Motz C 2015 *Mater. Charact.* **100** 178-91
[16] Gente C, Oehring M and Bormann R 1993 *Phys. Rev. B* **48** 13244–52
[17] Mackliet C A 1958 *Phys. Rev.* **109** 1964-70
[18] Arita M, Nakamura M, Goto K S and Ichinose Y 1984 *Pans. Jap. Inst. Met.* **25** 703
[19] Bruni F I and Christian J W 1973 *Acta Met.* **21** 385
[20] Neumann G and Tolle V 1986 *Phil. Mag. A* **54** 619-29
[21] Bussman W, Herzig C, Rempp W, Maier K and Mehrer H 1979 *Phys. Stat. Sol. (a)* **56** 87-98